Journal of Membrane Science 425–426 (2013) 141–148

Contents lists available at SciVerse ScienceDirect

Journal of Membrane Science

journal homepage: www.elsevier.com/locate/memsci

Transport through composite membranes, part 2: Impacts of roughness on permeability and fouling

Guy Z. Ramon [1], Eric M.V. Hoek *

Department of Civil & Environmental Engineering and California NanoSystems Institute, University of California, Los Angeles, CA, USA

ARTICLE INFO

Article history:
Received 12 January 2012
Received in revised form
31 July 2012
Accepted 1 August 2012
Available online 18 August 2012

Keywords:
Membrane
Composite
Reverse osmosis
Roughness
Fouling
Transport

ABSTRACT

Transport through composite membranes is influenced by the permeability and selectivity of the coating film and also by the skin layer pore morphology of the underlying porous support; however, the previous published research considered coating films with uniform thickness. Herein, we employed a numerical model to probe the impacts of coating film morphology on: (1) coating film permeability, (2) composite permeability, and (3) local permeate flux distribution. For the geometries modeled, coating film roughness can result in higher permeability provided that the mass of coating film is redistributed to produce both thinner and thicker cross-sections. On the other hand, permeability decreases when rough features are placed over a constant base film thickness. Further, rough coating films can exacerbate or dampen permeate flux 'hot spots' that appear over support membrane pores, depending on their relative orientation; however, dampening morphologies exhibit lower overall permeability even when the support membrane 'solid phase' is highly water-permeable. The presented theoretical results offer further insights into the fundamental challenges in designing high flux, fouling resistant RO membranes.

1. Introduction

Modern reverse osmosis (RO) membranes have composite structures, where a thin polymeric film is formed over a relatively thick, porous support membrane. Transport through the composite structure is largely dictated by the properties of the coating film; however, it is widely known that the support membrane impacts composite membrane transport. Previously, we formulated a theoretical model to probe the impacts on membrane transport imparted by the support membrane skin layer pore size, porosity and 'solid phase' microporosity, as well as coating film thickness [1]. Herein, we extend the model to consider a seemingly inherent feature of polyamide composite membranes formed by interfacial polymerization: surface roughness. The exact mechanisms leading to the formation of the typical 'ridge and valley' or lobe-like morphology characteristic of these surfaces (see Fig. 1 for representative images) are not entirely clear, but have been shown to correlate with reaction kinetics through monomer partitioning and diffusivity in the two-phase system used for the polymerization process, as well as the support physical and chemical properties [2–4].

Surface roughness has long been considered a cause of the high fouling propensity of modern polyamide-based composite RO membranes compared with earlier cellulose acetate-based membranes. Fouling studies have produced ample experimental evidence pointing at the correlation between roughness and fouling [5–8]. Various mechanistic explanations have been proposed, mostly focused on DLVO-type interfacial interactions and how these may be affected by surface roughness. In addition, there have been studies, which alluded to the possible correlation between higher flux and increased roughness, possibly due to an increased interfacial area between the rough membrane surface and the feed solution [9–13]. While fouling results seem fairly consistent (i.e., rougher membranes foul more quickly and are harder to clean), high permeability has been correlated with both increased and decreased roughness. Furthermore, surface morphology may alter the external mass transfer [3,12], creating another layer of complexity to the process, which is particularly important for transport of highly rejected solutes affected by external mass transfer conditions through concentration polarization.

The present study attempts to shed some light on the role that membrane morphology plays in transport through composite structures by applying the previously developed model to a few simplified geometrical representations, which capture the essential features of polyamide composite RO membrane surface

* Corresponding author at: University of California, Los Angeles, 5732 Boelter Hall, P.O. Box 951593, Los Angeles, CA 90095-1593, USA. Tel.: +1 310 206 3735; fax: +1 310 206 2222.
E-mail address: emvhoek@ucla.edu (E.M.V. Hoek).
[1] Present address: Department of Mechanical and Aerospace Engineering, Princeton University, Princeton, NJ 08540, USA.

0376-7388/$ - see front matter © 2012 Elsevier B.V. All rights reserved.
http://dx.doi.org/10.1016/j.memsci.2012.08.004

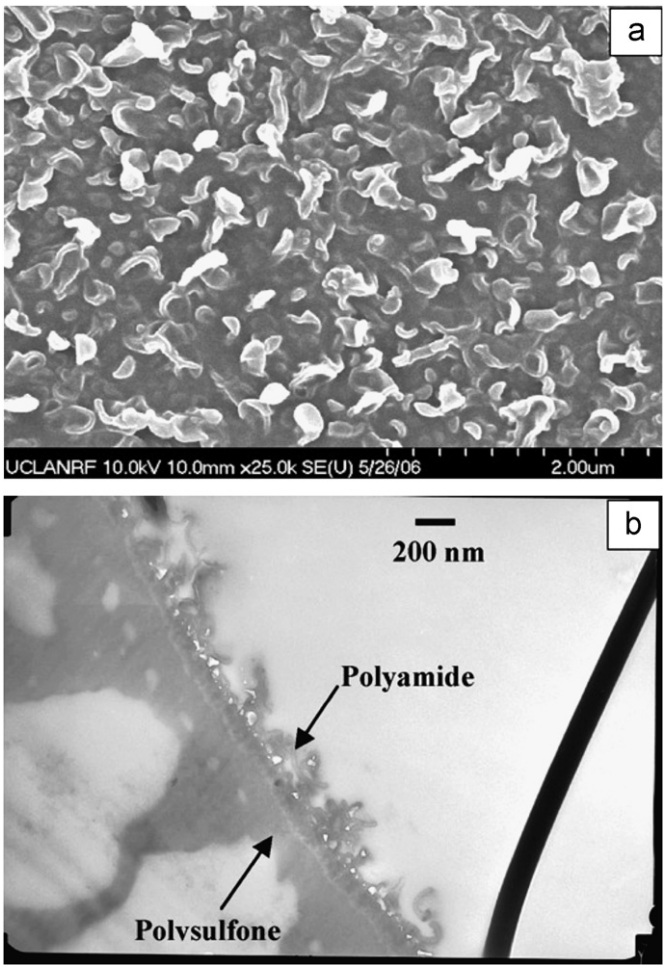

Fig. 1. Representative images, illustrative of the rugose morphology characteristic of polyamide thin-films constituting the top coating layer of a composite membrane. (a) SEM image of the film top surface. (b) TEM cross-section (Reproduced from Ghosh et al. [3].).

roughness. Simulations probe the interactions between rough coating films and the underlying porous support membrane pore morphology, with the specific goal of testing the following two hypotheses:

(1) Permeability increases with surface roughness if the roughness is created while producing thin regions in the coating film, essentially reducing the base film thickness; however, when roughness is formed on top of an unvarying base film thickness, the permeability of the film decreases with increased roughness.
(2) When surface roughness comes at the expense of base film thickness, the thinner regions ("valleys") present locally higher flux ("hot spots") than the thicker regions ("peaks"), and hence, these hot spots may be points of initiation for colloidal and organic deposition, as well as mineral scale formation.

This flux heterogeneity was previously suggested as a driver of colloidal fouling via "valley clogging", i.e., preferential deposition in valleys of rough polyamide composite RO membranes [7]. Finally, the model was used to illustrate possible ways in which coating film morphology and support membrane pore morphology may interact to dampen or exacerbate the magnitude of flux through hot spots.

2. Numerical model

The numerical model employed in the present study follows directly from that presented in the companion paper [1]; however, where the previous analysis considered smooth coating films, here we consider films with well-defined morphology used to simulate the roughness of polyamide composite RO membranes. We confine our analysis to 2D, since the previous results suggest minor deviations between 2D and 3D results. Briefly, the governing equation is the 2D Laplace equation, which describes the concentration field for steady-state diffusion through the coating film and underlying support material. The boundary conditions applied are identical to those described previously, namely a scaled potential (concentration) of unity at the interface between the coating film and feed solution, a potential of zero at the interface between the film and support pore, the continuity of diffusive flux at the interface between the film and support material solid phase and symmetry conditions where applicable (see supporting material in Appendix A for more detail about geometries, equations and boundary conditions).

In a first set of simulations probing the permeability of an unsupported film, roughness features on the coating film were modeled as rectangular, ellipsoid or sinusoidal (see schematic drawing in Fig. 2). Each unit cell is characterized by a base film thickness, the roughness amplitude (scaled against the base film thickness) and the surface coverage, ϕ, defined as the fraction of the unit cell surface occupied by the roughness feature (note that for the sinusoidal roughness unit, $\phi=1$ by definition). Numerical simulations were carried out, varying the roughness amplitude and coverage, while considering two possible scenarios. In the first, the base film thickness was kept constant, while in the second the total film 'mass' was conserved, such that when a roughness feature was enlarged, it was at the expense of the base film thickness. For each case, the flux at the feed/film interface was integrated and scaled against the flux obtained for a smooth film with unit thickness. This ratio was taken to be the scaled permeability, since the concentration difference across the film was equal to unity in all cases.

All other simulations were made using the sinusoidal geometry depicted in Fig. 2c, in which a membrane segment was constructed of a coating film with a sinusoidal thickness over a periodic porous support. With this geometry, the roughness amplitude was kept constant, while pore locations, number and size were varied; since these are periodic distributions, varying the pore number and location simulates different characteristic wavelengths and the relative phase of the roughness/pore distributions, or increased porosity at constant roughness wavelength. As before, the scaled permeability was calculated for each case as the ratio of the flux, integrated along the feed/film interface, to that of a smooth unsupported film. In order to present the flux distribution at the feed/film interface, the average flux was calculated by integrating along the film surface and was then used to scale the local flux.

The second set of simulations was undertaken with the goal of probing the way that a non-uniform morphology and underlying support structure interact to ultimately affect the permeability and the flux distribution at the membrane–feed interface. When simulating either film morphology or support structure, there are virtually limitless possibilities; however, a simple, periodic structure was chosen. While this constitutes an idealized version of reality, it nonetheless captures the essential behavior, at least qualitatively, while being easily illustrated and appreciated visually.

Available literature data suggests that typical RMS roughness features for a RO membrane are in the range of 50–180 nm [8,14,15]; average pore sizes of support membranes are in the range 5–30 nm [3,16] and surface porosity has been reported to be in the range 1–5% [16]. In light of these representative values, coating film geometries were modeled with a roughness amplitude of 100 nm, a wavelength (peak-to-peak separation) of 200 nm, a base film

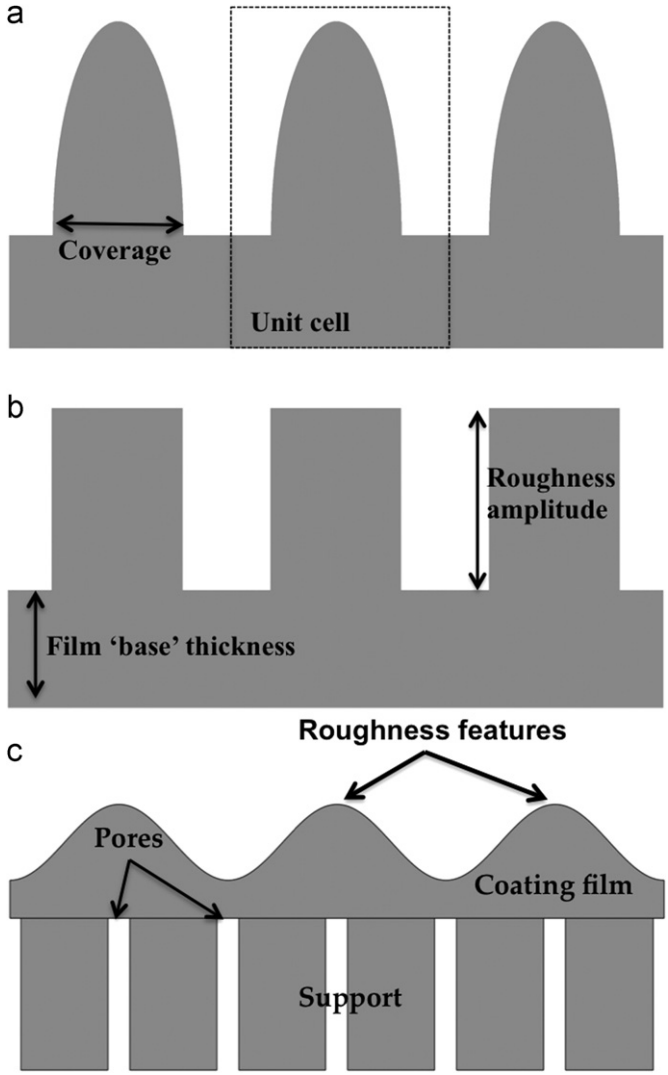

Fig. 2. Schematic drawings of the geometries employed for the numerical simulations. Roughness features were characterized, within a single unit cell, by an amplitude, scaled by the base film thickness, and a fractional surface coverage. (a) Ellipsoid. (b) Rectangular. (c) Membrane segment modeled as a coating film with sinusoidal roughness overlying a porous support material.

thickness of 50 nm (essentially an average of 100 nm, varying sinusoidally between 50 and 150 nm), while support membrane skin layers were modeled with pore diameters of 10 and 20 nm and porosities of 1% and 4%. As already noted, these idealized composite membrane geometries are not intended to reproduce actual properties of composite membranes; moreover, it is not clear that doing so would better achieve the goals of this investigation, due to the enormous computational requirements of modeling exact membrane morphologies. Therefore, relatively simple, representative membrane geometries were chosen to probe the impacts resulting from variations in film thickness, the size, number and location of support membrane pores and the relative locations of roughness features and support membrane pores.

3. Results and discussion

3.1. The impact of film morphology on permeability

We began by considering the following question: given an unsupported film, what would be the impact of a rougher surface on the film permeability? Considering the transport through the film to be purely diffusive and uniformly permeable (i.e., the film is uniformly dense and chemically homogeneous such that the solubility and diffusivity of a given species are everywhere equal), our simulations show that the permeability may either increase or decrease, depending on whether or not the roughness is at the expense of the film base thickness. This point is illustrated in Fig. 3, which clearly shows that if the base thickness is kept constant, roughness will only reduce the permeability. This effect will eventually saturate at some value of roughness, which is dependent on the extent of surface coverage (see Fig. 3a). In this case, roughness reduces the local concentration gradients, eventually leading to the roughness elements becoming mostly 'stagnant zones' through which very little transport occurs. Rectangular-shaped roughness presents a greater transport barrier than elliptical or sinusoidal elements, since (as simulated) they occupy more volume, and hence, produce larger reductions in local gradients. These results clearly illustrate that increased surface area, occurring in all cases where roughness is present, does not necessitate increased permeability. In other words, rougher membranes are not necessarily more permeable even when there is no change to membrane structure (i.e., permeable void volume when swollen with water). On the other hand, when the roughness is generated at the expense of the total film mass (or volume, since the film density is assumed to be everywhere constant), permeability increased. When the film was redistributed as a thinner base film with larger amplitude features, permeability increased with increasing roughness (see Fig. 3b). A larger increase was observed for rectangular elements since such a geometry represents a greater mass subtracted from the base film per unit increase in roughness amplitude.

This set of simulations, while an obviously crude idealization, provides a theoretical basis for the following practical observation. For a constant membrane structure, roughness can only increase permeability if for every increase in film thickness there is a proportionate decrease. This is a simple consequence of the diffusive nature of membrane transport (as simulated) and cannot be explained as the result of increased interfacial area. During the revision of this paper, it has come to our attention that this conclusion had been independently reached using similar theoretical arguments [17], which compared well with experimental measurements for an unsupported gas-separation membrane prepared with rectangular roughness features [13].

Published AFM data suggests that the extent to which roughness elements protrude above the lowest point measured (equivalent to the top of the 'base film' here) may vary widely, depending on the type of membrane. In extreme cases, this can be up to ~1 μm [14]; however, on average these values appear to vary between 50 nm and 300 nm for a range of RO membranes [8,14,15]. From SEM and TEM images (e.g., Fig. 1 and [3,4]), base film thickness range from 20 to 100 nm; hence, the scaled roughness, as defined here, is typically greater than unity, on average, and can locally be greater than ~10. However, it is difficult to directly attribute changes in permeability solely to roughness for interfacially polymerized polyamides because different morphologies also may reflect different local compositions and extents of cross-linking; such spatial heterogeneity of the polymer suggests that the transport properties may also vary spatially.

3.2. Roughness and support pores create localized flux 'hot spots'

In the companion paper [1] it was shown how confinement of transport out of the coating film into the support pores results in an uneven flux distribution at the coating film/feed interface. This effect is particularly pronounced for a thin coating film over a low

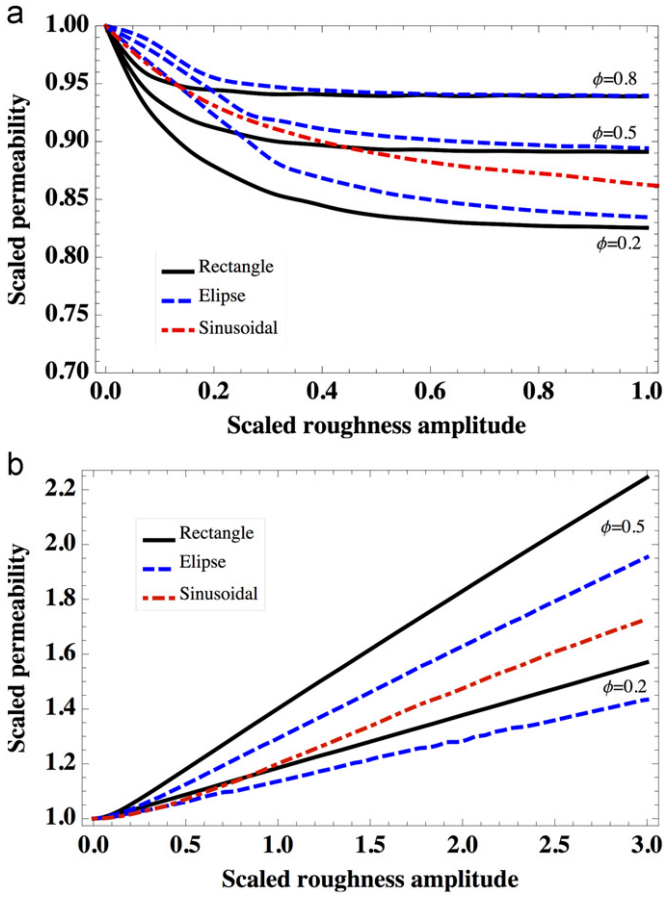

Fig. 3. Effect of roughness features with varying surface coverage (ϕ) and amplitude (scaled against the base film thickness), on the permeability of the thin-film, scaled against the permeability of a smooth film for (a) Constant base film thickness. (b) Constant film mass. In both cases, the roughness amplitude is scaled with the base film thickness.

porosity support, and when the support solid phase has a low permeability relative to the coating film. The flux distribution may vary to the extent that some fraction of the membrane is effectively excluded from transport, while in other regions the flux may be several times higher than the average flux through the membrane.

A similar effect is expected to emerge when considering the flux over a film of spatially varying thickness. Fig. 4 shows a few representative membrane segments with the calculated concentration field and diffusive flux streamlines through the coating film, overlaid by the flux distribution, scaled against the average flux calculated over the entire segment. Note that in these, the support solid phase is taken to have very low permeability and so transport out of the film is confined to the pores of the support. As already discussed previously, the geometry here was chosen so as to illustrate the main features affecting transport and is certainly not exhaustive of the innumerable possible combinations.

In the first two cases, shown in Fig. 4a and b, the pore distribution and roughness are taken to have an equal wavelength, that is, the characteristic scale of the pore-to-pore separation is of similar magnitude as the peak-to-peak distance of the roughness. However, two extreme cases of alignment, or phase, are considered: one in which pores are located directly under valleys ('in-phase') or vice-versa, pores out-of-phase with roughness, located under peaks. As may be seen, in-phase pore locations (Fig. 4a) result in a highly localized flux distribution; the peak flux, in the case considered, is four times higher than the average flux, compared with ~1.3 for the non-aligned case (Fig. 4b). It must also be noted that the reduction in the magnitude of these 'hot spots' is at the expense of the scaled permeability, which is reduced from 0.44 to 0.28 (this is the permeability ratio taken against a flat, unsupported film with the same average thickness). Next, we consider the effect of changing the porosity (in this case, increasing from ~1% to ~4%) by either increasing the number of pores or their size, the former being identical to increasing the characteristic roughness wavelength. In the case of increased pore number, two cases are again considered for the relative alignment (i.e., in and out-of-phase). As may be seen in Fig. 4c and d, increasing the relative number of pores (reducing the confinement) produces a more even flux distribution, as does increasing pore size (Fig. 4e).

3.3. Minimizing hot spots by roughness-induced 'wave interference'

While the present analysis does not presume to produce real values of fluxes or permeabilities, it illustrates general trends and features of the complex interplay between rough coating films and underlying support membrane pore morphology. The most important feature is the localized 'hot spots' with high flux relative to the area average flux one would observe experimentally (or at a real RO plant). The hot spots seem to be an inherent feature of rough, composite membranes, and are expected to serve as initiation points for scaling and fouling due to the locally elevated concentration polarization and permeation drag, respectively. It is therefore instructive to consider the possible combinations, which may act to reduce the occurrence of these local flux peaks. In principle, the uneven flux distribution, generated separately by the roughness and pores, interacts in a manner that is somewhat reminiscent of wave interference; for example, there will be an additive effect when pores are aligned with roughness minima—these are locations of local flux peaks in the respective distributions. This effect is clearly observable in Figs. 5 and 6, where the flux distributions are shown, separated into their constituents, i.e., the distribution in the case of no support membrane pore confinement, a smooth film over a support and the two cases combined. In Fig. 5 these distributions are shown over the representative membrane segment containing both aligned and non-aligned pore contributions, and the flux is scaled against the average flux calculated over the same segment. Fig. 6 shows a similar break-down of the contributions to flux variations, this time for strictly aligned (Fig. 6b) and non-aligned (Fig. 6c) pore locations; here the flux is scaled against that of a smooth, unsupported film, so as to illustrate the trade-off between the permeability and dampening of the flux distribution. Despite the linearity of the governing equation, the separate pore/roughness effects are not simply additive since mapping these two solutions (of a linear PDE) onto the same domain would require a non-linear transformation due to the sinusoidal morphology.

What these plots do tell us is that, since the roughness and pore distributions are probably random for a realistic membrane, one might expect to find regions where pore locations (note that these may very well be 'clusters of pores', over regions on the scale of a few micrometers in size or more) correspond with a locally thin coating film (roughness minima), generating a flux peak or, conversely, a stagnant region. However, it may be possible and is certainly desirable to dampen this uneven flux distribution. Increasing the support porosity may be one possible route towards dampening the uneven flux distribution; it was previously shown that a thick film will also dampen the flux peaks, but this will also invariably reduce the overall permeability.

Another possibility, illustrated in Fig. 7, is to consider the transport through the solid phase of the support material. In the

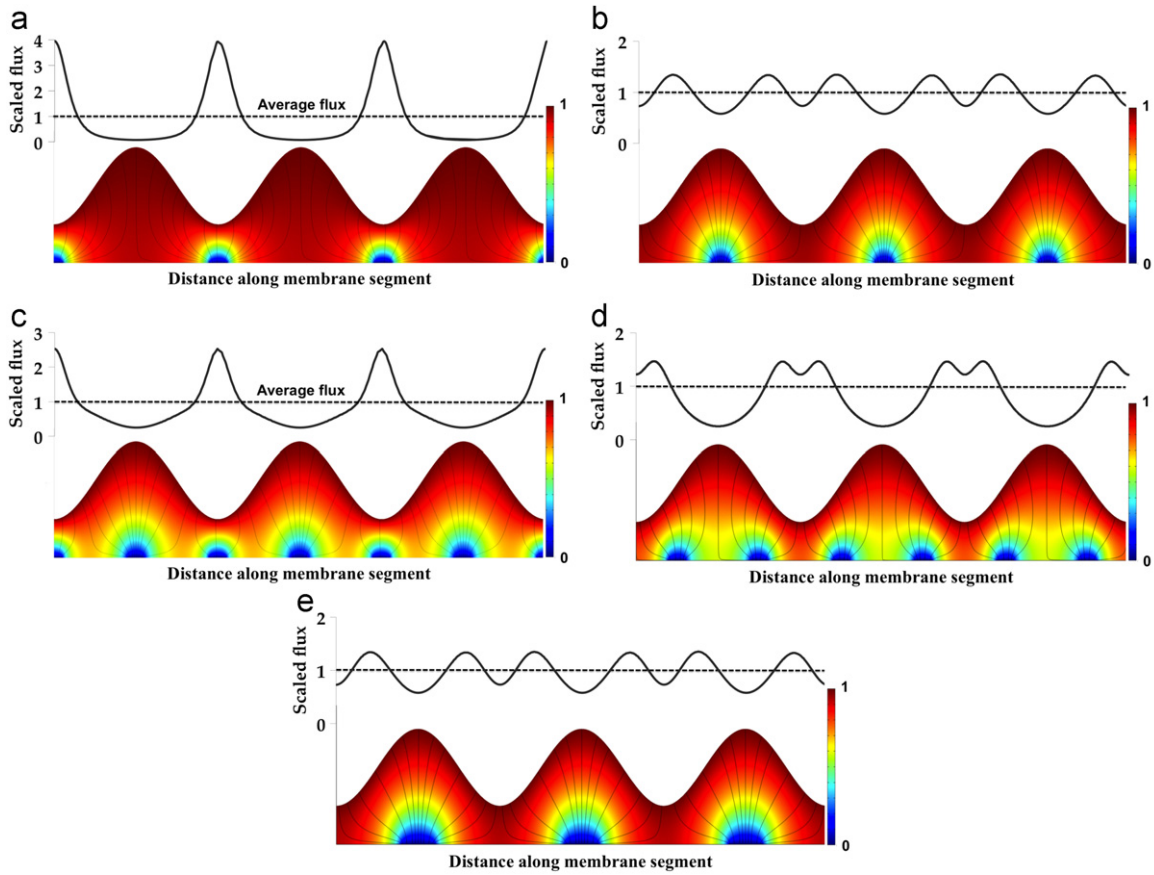

Fig. 4. Simulated membrane segments over a porous support with an impermeable solid phase, showing the concentration field and diffusive streamlines emerging under the combined effect of film roughness and support pores. Overlaying each segment is the local distribution of the water flux through the membrane, scaled against the average flux integrated along the segment. (a) Equal wavelength, aligned (in-phase) roughness and support pore distribution. (b) Equal wavelength, non-aligned (out-of-phase) roughness and pore distributions. (c) Roughness with a double wavelength or, equivalently, double porosity of the support skin layer, in-phase. (d) Same as (c), out-of-phase. (e) Out-of-phase, equal wavelength, double sized pores.

cases shown, aligned (Fig. 7a) and non-aligned (Fig. 7b), double porosity (or wavelength) supports are also assigned a permeant diffusion coefficient (in the "solid" phase of the support, which is really microporous) that is identical to that of the coating film. The flux distribution is dampened when the microporosity of the support membrane offers diffusion equal to that of the coating film; however, we have not accounted for any differences in solute or solvent partitioning into the support membrane microporous regions. The original cellulose acetate integrally skinned RO membranes represent a case where the solubility and diffusivity of solvent and solutes should be roughly the same throughout the microporous regions of the skin layer and supporting layer.

As may be seen in Fig. 8, when the support provides an additional path for diffusion, the resulting flux distribution is dampened; as before, a non-aligned porosity (Fig. 8b) produces a greater dampening effect. Intuitively, we can expect the characteristics of the composite to approach those of the isolated thin-film, at the limit where the support is completely permeable and poses no transport limitations. In the case where the pores and roughness are aligned (Fig. 8a), increasing the relative diffusivity in the support, D_s, significantly dampens the peak flux, and when the support solid is 10 times more permeable than the film material, the resulting flux distribution becomes practically identical to that of the isolated film. In the non-aligned case, the opposite is true—the peak flux increases as the support becomes more permeable; this may be attributed to the strong dampening offered by the non-aligned arrangement of pore confinement, which is now relaxed. In addition, the location of the peaks shifts to correspond with the roughness, whose contribution now dominates the flux distribution.

3.4. The trade-off between flux, rejection and hot spots

The results previously discussed and the physical insight they provide raise the question of how these different contributions to an uneven flux distribution may be manipulated so as to produce a minimal number of high fouling propensity 'hot spots'. Specifically, it is apparent that there may be a competition between making a highly permeable membrane while maintaining a relatively even flux distribution. One might conclude that high flux membranes (of this type) must be inherently rough, and therefore, inherently fouling prone; however, it may be possible to overcome this paradigm by increasing the permeability (microporosity) of the support membrane solid phase. Based on previous results, we know that the support may significantly reduce the permeability of the composite membrane; we also know that there is a possible interplay between pore size and total porosity through which flux and rejection may be fine-tuned [1]. It seems one must seek out the most appropriate compromise between permeability and fouling propensity, but this may also change the rejection properties. Eliminating the effect of the support by making it more permeable will certainly raise the overall permeability, however, this would also eliminate the degrees of freedom offered by the support properties, which seem to enable rejection to be fine-

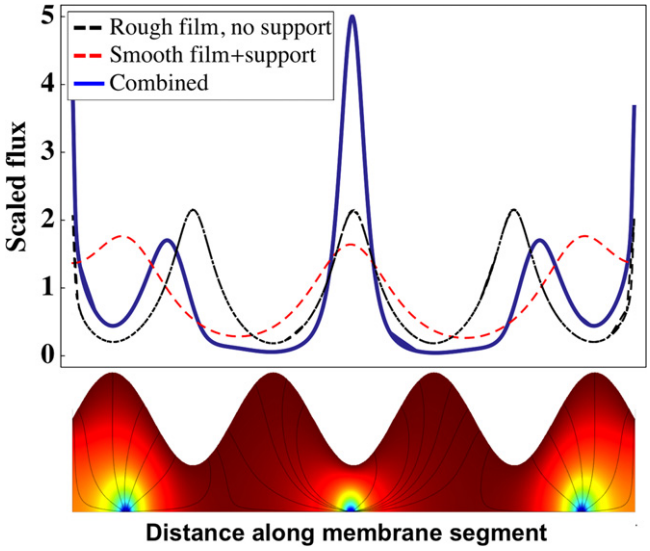

Fig. 5. Flux distribution over a simulated membrane segment, scaled by the average flux integrated along the segment, showing the emerging distribution as affected by the support pores (for a flat film), the roughness features (with no support) and the combined 'wave interference' of both effects.

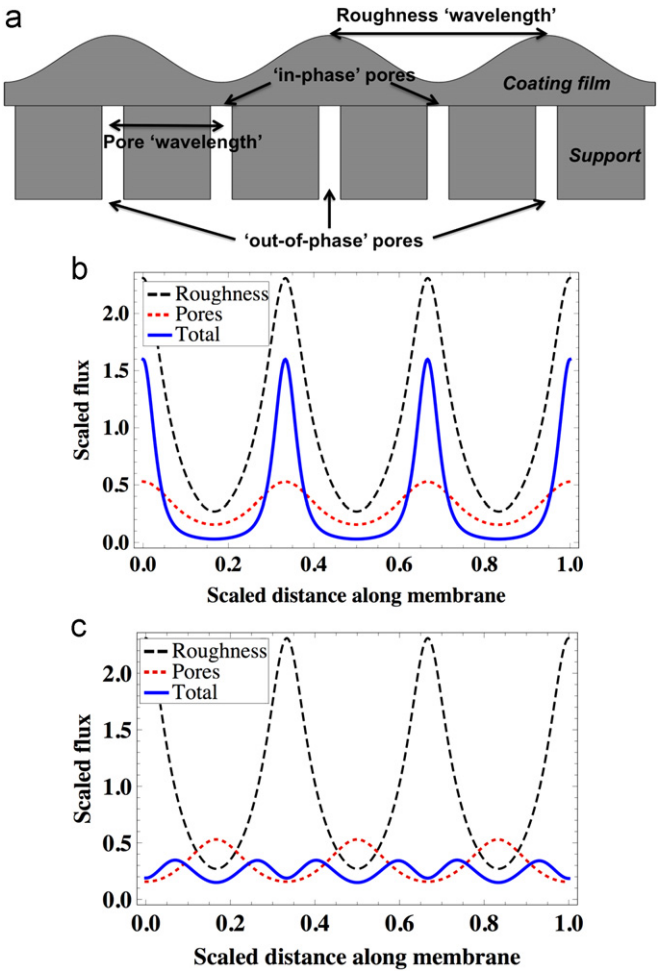

Fig. 6. Flux distribution over a simulated membrane segment, scaled by the flux calculated for an undisturbed film (i.e., a smooth film with no underlying support), showing the emerging distribution as affected by the support pores (for a flat film), the roughness features (with no support) and the combined 'wave interference' of both effects. (a) Illustrative schematic of roughness and pore relative alignment. (b) Equal pore and roughness wavelength, in-phase distributions. (c) Equal pore and roughness wavelength, out-of-phase distributions.

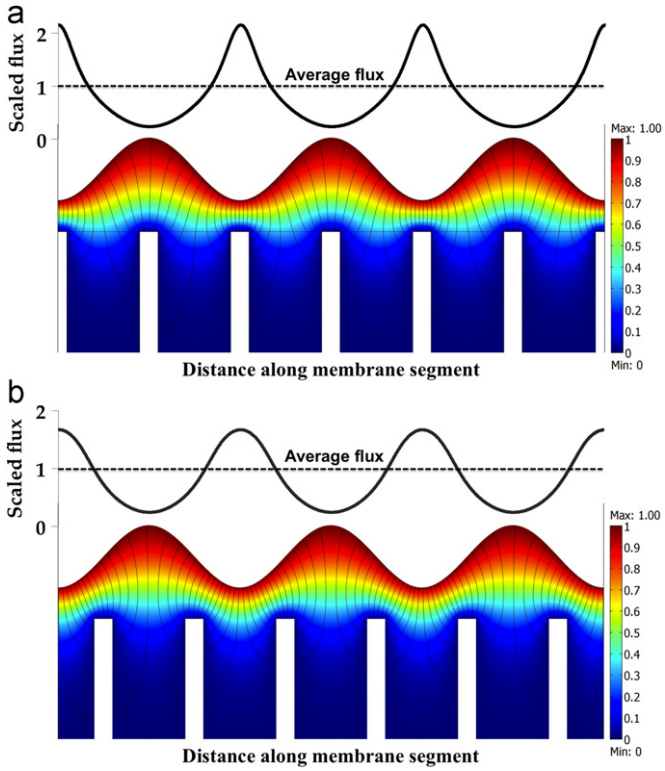

Fig. 7. Representative simulations of membrane segments over a porous support with a permeable solid phase (set to be equally permeable as the coating film) showing the concentration field and diffusive streamlines emerging under the combined effect of film roughness and support pores. Overlaying each segment is the local distribution of the water flux through the membrane, scaled against the average flux integrated along the segment. (a) Double wavelength roughness, aligned (in-phase) with support pore distribution. (b) Double wavelength roughness, non-aligned (out-of-phase) with pore distribution. *Note:* the color-coding for the concentration ranges from 1 (red) to zero (blue). (For interpretation of the references to color in this figure caption, the reader is referred to the web version of this article.)

tuned independently of material chemistry. In Fig. 9, the general trends observed in our simulations are summarized for each case considered. Specifically, the permeability shown is scaled against that of an isolated smooth film, in addition to the peak flux relative to the average flux. The charts are separated so as to differentiate between the general scenarios, namely the separate effects of coating film roughness and support membrane pores (Fig. 8a), the case of an impermeable support solid material (Fig. 8b) and the case of a support solid in which the permeating species' diffusivity is equal to that in the coating film (Fig. 8**c**).

Based on these figures, the following observations may be made, some of which re-iterate previously discussed notions. Making a film rougher will increase its permeability if proportional cross-sections of the film decrease in thickness to enable other cross-sections to increase in thickness. Having a support membrane always reduces permeability, unless it has a highly porous skin layer and its solid phase exhibits microporosity and structure that permit transport comparable to or greater than the overlying coating film. Perhaps the most promising strategy for tailoring composite membrane transport is the fabrication of support membranes with highly porous skin layers with small pores, preferably made from a material whose transport properties are comparable to those of the film. However, this would mean there might be an inherent compromise in terms of the achieved rejection, since our previous results also suggest that in order to maximize rejection, large pores and low porosity are desirable.

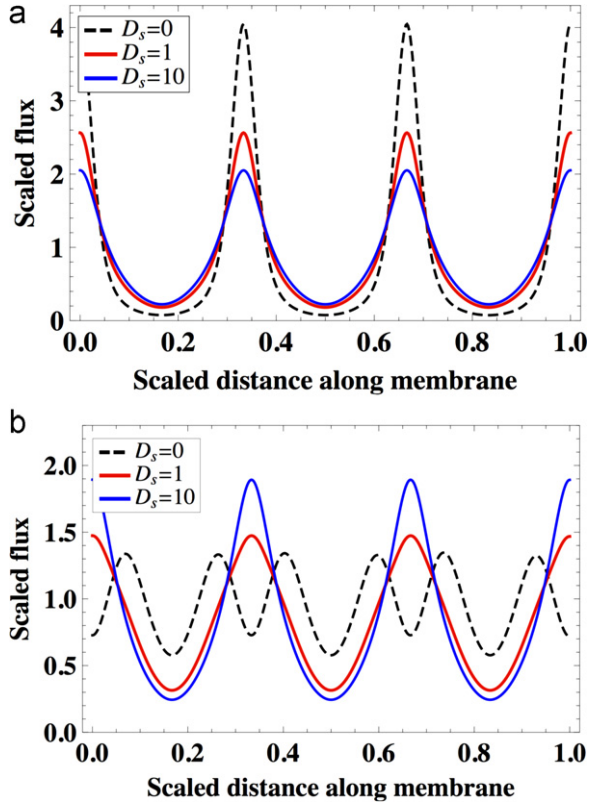

Fig. 8. Effect of support solid phase permeability on flux distribution along the membrane segment, shown for different values of D_s, the permeating species diffusivity within the support relative to that in the coating film. (a) Equal wavelength, aligned (in-phase) roughness and support pore distributions. (b) Equal wavelength, non-aligned (out-of-phase) roughness and support pore distributions. *Note:* see Fig. 6a for schematic illustration of pore vs. roughness alignment and definitions.

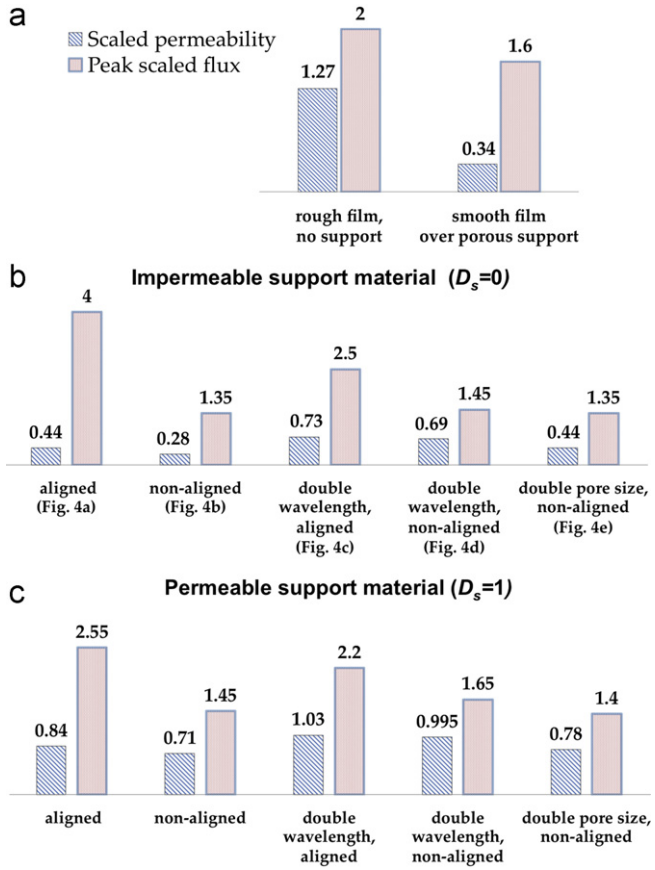

Fig. 9. Comparison of the various simulated scenarios, showing the permeability, scaled against that of an equivalent, smooth film with no underlying support structure, and the peak flux. (a) Base cases showing the individual contributions of the roughness and support pores. (b) Impermeable support material (note each case references the corresponding case shown in Fig. 4. (c) Support material with diffusivity equal to that of the coating film. *Note:* Aligned ('in-phase') and non-aligned ('out-of-phase') denote pore locations underneath roughness minima and maxima, respectively; double wavelength refers to the typical peak-to-peak distance of the surface toughness, compared with an average pore-to-pore separation distance in the support skin layer (see Fig. 6a for a schematic illustration).

4. Concluding remarks

Simplified model geometries accounting for typical polyamide coating film roughness features and polysulfone support membrane pore morphologies were used to simulate diffusive transport through composite RO membranes. These simulations provide an understanding of both intuitive and non-intuitive interactions that conspire to govern transport characteristics of composite RO membranes. Specifically, the flux distribution that emerges may further govern the fouling propensity of modern RO membranes through hot spots with greatly elevated local water fluxes. It appears theoretically possible to dampen hot spots while minimizing the loss of overall permeability by (1) controlling periodicity and alignment of roughness features relative to support membrane pores, (2) preparing support membranes with high skin layer porosity and small pores, and (3) preparing support membranes whose solid phase offers similar transport characteristics to those of the coating film. This suggests another explanation, beyond their low permeability, smooth interface and super-hydrophilicity, why integrally skinned cellulose acetate RO membranes almost universally appear more fouling resistant than composite polyamide RO membranes. As a final note, the presented results suggest that if the strategy for making a 'high flux' membrane is through formation of a rough coating film, then the resulting membrane will be inherently fouling prone, but this is a purely hydrodynamic perspective; a complete understanding must also include DLVO-type interfacial interactions.

Acknowledgments

G.Z.R. was supported by a Vaadia-BARD Postdoctoral Fellowship, Award no. FI-435–2010 from BARD, The United States—Israel Bi-national Agricultural Research and Development Fund and a Marie-Curie Fellowship under the FP7 program of the European Research Council.

Appendix A. Supporting information

Supplementary data associated with this article can be found in the online version at http://dx.doi.org/10.1016/j.memsci.2012.08.004.

References

[1] G.Z. Ramon, M.C.Y. Wong, E.M.V. Hoek, Transport through composite membranes. part 1: is there an optimal support membrane? J. Membr. Sci. 415–416 (2012) 298–305.
[2] P.W. Morgan, S.L. Kwolek, Interfacial polycondensation. II. Fundamentals of polymer formation at liquid interfaces, J. Polym. Sci. 40 (1959) 299–327.
[3] A.K. Ghosh, B.-H. Jeong, X. Huang, E.M.V. Hoek, Impacts of reaction and curing conditions on polyamide composite reverse osmosis membrane properties, J. Membr. Sci. 311 (2008) 34–45.

[4] A.K. Ghosh, E.M.V. Hoek, Impacts of support membrane structure and chemistry on polyamide–polysulfone interfacial composite membranes, J. Membr. Sci. 336 (2009) 140–148.
[5] M. Elimelech, X. Zhu, A.E. Childress, S. Hong, Role of membrane surface morphology in colloidal fouling of cellulose acetate and composite aromatic polyamide reverse osmosis membranes, J. Membr. Sci. 127 (1997) 101–109.
[6] X. Zhu, M. Elimelech, Colloidal fouling of reverse osmosis membranes: measurements and fouling mechanisms, Environ. Sci. Technol. 31 (1997) 3654–3662.
[7] E.M. Vrijenhoek, S. Hong, M. Elimelech, Influence of membrane surface properties on initial rate of colloidal fouling of reverse osmosis and nanofiltration membranes, J. Membr. Sci. 188 (2001) 115–128.
[8] E.M.V. Hoek, S. Bhattacharjee, M. Elimelech, Effect of membrane surface roughness on colloid-membrane DLVO interactions, Langmuir 19 (2003) 4836–4847.
[9] M. Hirose, H. Ito, Y. Kamiyama, Effect of skin layer surface structures on the flux behaviour of RO membranes, J. Membr. Sci. 121 (1996) 209–215.
[10] S.Y. Kwak, D.W. Ihm, Use of atomic force microscopy and solid-state NMR spectroscopy to characterize structure-property-performance correlation in high-flux reverse osmosis (RO) membranes, J. Membr. Sci. 158 (1999) 143–153.
[11] S. Madaeni, The effect of surface characteristics on RO membrane performance, Desalination 139 (2001) 371–371.
[12] S. Al-Jeshi, A. Neville, An investigation into the relationship between flux and roughness on RO membranes using scanning probe microscopy, Desalination 189 (2006) 221–228.
[13] A.M. Peters, R.G.H. Lammertink, M. Wessling, Comparing flat and micropatterned surfaces: gas permeation and tensile stress measurements, J. Membr. Sci. 320 (2008) 173–178.
[14] S.Y. Kwak, S.G. Jung, Y.S. Yoon, D.W. Ihm, Details of surface features in aromatic polyamide reverse osmosis membranes characterized by scanning electron and atomic force microscopy, J. Polym. Sci. B: Polym. Phys. 37 (1999) 1429–1440.
[15] C.Y. Tang, Y.N. Kwon, J.O. Leckie, Effect of membrane chemistry and coating layer on physiochemical properties of thin film composite polyamide RO and NF membranes II. Membrane physiochemical properties and their dependence on polyamide and coating layers, Desalination 242 (2009) 168–182.
[16] G.R. Guillen, T.P. Farrell, R.B. Kaner, E.M.V. Hoek, Pore-structure, hydrophilicity, and particle filtration characteristics of polyaniline–polysulfone ultrafiltration membranes, J. Mater. Chem. 20 (2010) 4621–4628.
[17] C.E. Goodyer, A.L. Bunge, Mass transfer through membranes with surface roughness, J. Membr. Sci. 409–410 (2012) 127–136.